Polymer Properties of Polythymine as Revealed by Translational Diffusion

Sören Doose, Hannes Barsch, and Markus Sauer
Applied Laser Physics and Laser Spectroscopy, University of Bielefeld, Bielefeld, Germany

ABSTRACT Biopolymers, such as single-stranded DNA (ssDNA), are often described as semiflexible polymers or wormlike chains. We investigated the length dependence of diffusional properties of homogeneous ssDNA (polythymine) with up to 100 nucleotides using fluorescence correlation spectroscopy. We found that the hydrodynamic radius R_h scales according to a power law, with an exponent between 0.5 and 0.7 depending on ionic strength I. With R_h being proportional to the square root of the persistence length L_p, we found that $L_p \approx I^m$, with $m = -0.22 \pm 0.01$ for polythymine with 100 residues. For comparison, we performed molecular dynamics (MD) simulations with a force field that accounts for short-range interactions in vacuum, and determined the characteristic polymer properties end-to-end distance R, radius of gyration S, and persistence length L_p of various labeled and nonlabeled polythymine derivatives. We found excellent agreement for the length dependence of simulated S and experimental R_h measured at 100 mM NaCl, revealing that electrostatic interactions are completely shielded in aqueous solution at such ionic strength. MD simulations further showed that polythymine with $>\sim$30 residues can be described as a semiflexible polymer with negligible influence of the fluorescent label; and that static flexibility is limited by geometrical and steric constraints as expressed by an intrinsic persistence length of $\sim$1.7 nm. These results provide a benchmark for theories and MD simulations describing the influence of electrostatic interactions on polyelectrolyte properties, and thus help to develop a complete and accurate description of ssDNA.

INTRODUCTION

Our understanding of biopolymers, such as polynucleotides, polypeptides, actin filaments, or microtubules, has greatly benefited from standard polymer theory (1–5). Dynamic as well as static flexibility (3) of polynucleotides and polypeptides have been investigated using a broad range of experimental techniques. Biopolymers that are stiff on length scales above the dimension of individual monomers display polymer characteristics that are weakly dependent on the molecular structure at the atomic level. Double-stranded DNA (dsDNA), for example, was found to be a model polyelectrolyte (charged polymer chain), with structural and dynamic properties in very good agreement with those of an ideal polymer. Description as a wormlike chain (WLC) yields quantitative parameters for static flexibility (6,7). Most important, the length scale on which a biopolymer becomes flexible can be described by the persistence length, and it was found to be $\sim$50 nm for dsDNA (7–9), $\sim$15 μm for actin filaments (10,11), and $\sim$5 mm for microtubules (12,13), to name a few. Unstructured single-stranded polynucleotides (ssDNA, RNA) (7,14–18) or unstructured peptides (19–21) exhibit a much shorter persistence length of a few nanometers or less.

Several contributions have been identified that play an essential role in determining allowed polymer conformations and conformational dynamics: 1), the monomer structure providing degrees of freedom in the polymer backbone due to rotation around atomic bonds; 2), steric restrictions due to the presence of side groups; and 3), hydrophobic and electrostatic interactions between side groups or side groups and backbone. These short-range (van der Waals), as well as long-range (electrostatic), interactions can strongly influence the persistence length and/or induce so-called excluded-volume effects due to impenetrability upon folding of the polymer on itself, and thus have to be accounted for in a detailed description of real polymers. (Throughout this work, we will make the distinction between short- and long-range interactions with respect to the length scale over which physical forces extend. This is in contrast to the notion of Flory and others, who differentiate between short- and long-range interactions depending on the distance between interacting polymer segments, such that restricted orientations of neighboring bonds are due to short-range interactions and excluded-volume effects represent long-range interactions.) Deviations from simple polymer behavior have been particularly important for dilute polyelectrolyte solutions, in which solvated ions can shield electrostatic interactions and polymer properties become dependent on the ionic strength of the solvent. The electrostatic influence has been expressed, originally in Odijk-Skolnick-Fixman (OSF) theory, through an apparent persistence length L_p that consists of an intrinsic L_{p0} and an electrostatic component L_{pe}: $L_p = L_{p0} + L_{pe}$ (22,23). The accurate scaling behavior of L_{pe} as a function of ionic strength I has been predicted to be between $\sim I^{-1}$ (22–24) and $\sim I^{-0.5}$ (25,26), depending on specific values for the intrinsic flexibility, the strength of electrostatic interactions, and the charge density along the polymer. However, no satisfying theory has been developed

Submitted February 21, 2007, and accepted for publication April 12, 2007.

Address reprint requests to Sören Doose, Applied Laser Physics and Laser Spectroscopy, University of Bielefeld, 33615 Bielefeld, Germany. E-mail: sdoose@physik.uni-bielefeld.de.

Editor: David P. Millar.

0006-3495/07/08/1224/11 $2.00

doi: 10.1529/biophysj.107.107342

that covers all situations, in particular the situation that is valid for ssDNA in aqueous solution (27,28).

Because polymer properties, such as average square end-to-end distance, radius of gyration, or persistence length, are deduced from experimental results by applying a certain polymer model, it is important to verify accordance with the model. Based on Flory's seminal work on polymer conformations, Flory, Olson, and co-workers have shown that a polypeptide, as well as a polynucleotide, chain can be well described as an equivalent freely rotating chain (i.e., a freely jointed chain (FJC) with reduced flexibility due to constrained bond angles) with a well defined virtual bond of constant length (1,14,15,29,30). Description as a continuous WLC, which is the equivalent for long chains, has also been applied, and becomes more appropriate when the contour length of the investigated polymer is of a size comparable to or smaller than the persistence length.

Experimental techniques used to deduce properties of biopolymers include force-extension measurements, NMR, light scattering, video imaging, atomic force microscopy, and various methods to measure translational and rotational diffusion constants. As diffusion of polynucleotides is important for a variety of molecular processes (mobility of nucleotides in the cytoplasm; nuclear uptake of nucleotides in the cell; separation of DNA fragments by electrophoresis or Brownian ratchets (31)), the diffusion constant of dsDNA has been investigated for all size regimes from well below to well above the persistence length. The translational diffusion constant most often is a well defined function of the radius of gyration S. Simple scaling laws for the length dependence of S were found in dsDNA (7,32) and denatured proteins (33,34) in accordance with polymer theory (1,4). S was found to scale with polymer length following a power law with an exponent between 0.5 and 0.6, provided the contour length is much larger than the persistence length (35). For comparison, an exponent of 0.5 is predicted for an ideal polymer, increasing to 0.588 when excluded-volume effects are taken into account (1,36). Theoretical predictions, and some experimental evidence for a WLC with the contour length on the same order as the persistence length, suggest scaling behavior with a larger exponent (2,36–38). Diffusion of rodlike polymers in which the contour length is much smaller than the persistence length, e.g., short double-stranded DNA, has also been studied extensively by experimental and theoretical means (39–42).

Experimental observations of diffusion constants for both ssDNA and polypeptides, on the other hand, are sparse, and a precise length scaling of S for ssDNA with <100 residues has not been reported yet. Salt-dependent changes in structure and dynamics of ssDNA have been observed for circular plasmids and viral DNA by dynamic light scattering (43,44), for short polythymines with a few tens of residues by single-molecule Förster resonance energy transfer (FRET) (17,45) or birefringence measurements (16), and for ssDNA with several thousand residues by force-extension measurements (7,46). Dessinges et al. have shown that the description of long, heterogeneous ssDNA as a FJC or WLC model is not quite accurate at low extension in arbitrary salt conditions, most likely due to electrostatic self-avoidance inducing excluded-volume effects and base-pairing or stacking interactions (46–48). Murphy et al. have extracted a salt-dependent persistence length for ssDNA by comparing FRET measurements of average end-to-end distances with predictions of a WLC model (17). Their analysis relied on the fact that short homonucleotides made of thymine residues exhibit negligible base-pairing or stacking interactions and that a WLC description is appropriate. Average square end-to-end distances $\langle R^2 \rangle$ are also of interest in the context of end-to-end contact kinetics. Recently, a simple scaling law, $k \sim n^b$, for end-to-end contact rates k and polymer length n, was revealed for both unstructured peptides (49,50) and ssDNA (S. Doose, J. Kim, H. Neuweiler, and M. Sauer, unpublished data; 52) with tens of residues ($b = -1.5$ to -2.1 for either biopolymer). As theory predicts a precise scaling law as a function of $\langle R^2 \rangle$, it is necessary to know the accurate length dependence of $\langle R^2 \rangle$ for validation. Also, the question remains as to how well a WLC (FJC) model resembles a real polynucleotide, in particular at short length scales.

In this work, we compare experimental diffusion constants of polythymine with polymer properties derived by computer simulation. We use fluorescence correlation spectroscopy (FCS) to observe translational diffusion of polythymine labeled with the oxazine derivative MR121 (MR121-$(dT)_N$, with $N = 5$, 10, 20, 40, 80, and 100) and determine the dependence of diffusion constants on polymer length and ionic strength. To estimate alteration of diffusion constants by the fluorescent label, we performed molecular dynamics (MD) simulations for labeled and unlabeled polythymine. MD simulations were performed in vacuum with a force field limited to short-range van der Waals interactions resembling a hard-sphere potential, thus taking geometrical and sterical constraints into account. The aim of this work is to characterize polymer properties specifically in the context of polythymine using simulated and measured diffusion experiments, and to compare the results with standard polymer models. We investigate static properties, such as end-to-end distance, radius of gyration, and persistence length as a function of polymer size. A comparison between experimental and computational results shows that polythymine can be reasonably well described by a WLC model for $>\sim 30$ residues. We estimate an intrinsic persistence length and investigate experimentally how the electrostatic interaction changes the persistence length as a function of ionic strength.

MATERIALS AND METHODS

DNA samples

Synthetic oligonucleotides of polythymine $(dT)_N$ with $N = (5, 10, 20, 40, 80, 100)$ were purchased from IBA (Göttingen, Germany). The fluorescent

oxazine dye MR121 (53) was kindly provided by K. H. Drexhage (ATTO-TEC, Siegen, Germany). The 5′-ends of polythymine were labeled with MR121 via an aliphatic C3 amino modifier using classical *N*-hydroxysuccinimidylester (NHS-ester) chemistry. Labeling was performed in phosphate-buffered saline containing 10% (v/v) carbonate buffer (100 mM, pH 8.5). A fivefold molar excess of NHS ester was added to 15–20 nM oligonucleotide and incubated for 2 h at room temperature in the dark. Fluorescently modified oligonucleotides were purified using reverse-phase (Hypersil-ODS column) HPLC (Agilent Technologies, Waldbronn, Germany). Separation was performed in 0.1 M triethylammonium acetate, using a linear gradient from 0 to 75% acetonitrile in 20 min.

Fluorescence correlation spectroscopy

All FCS measurements were performed on a home-built confocal microscope, as described elsewhere (54). MR121 was excited at 632.8 nm (50 μW measured at the back aperture of the objective) using a HeNe laser. Photobleaching was not detectable at the chosen excitation power. The collimated laser beam was coupled into an oil-immersion objective (63×, NA 1.4, Zeiss, Oberkochen, Germany) by a dichroic beam splitter (645DRLP, Omega Optical, Brattleboro, VT). The fluorescence signal was collected by the same objective, filtered by a bandpass filter (700DF75, Omega Optical), separated into two beams using a cubic nonpolarizing beamsplitter (Linos, Göttingen, Germany), coupled into multimode optical fibers with a diameter of ~100 μm, and imaged onto the active area of two single-photon avalanche photodiodes (APDs, AQR-14, PerkinElmer, Fremont, CA). The signals of the APDs were cross-correlated (15 min for each measurement) using a digital real-time multi-τ correlator device (ALV-6010, ALV, Langen, Germany) with a time resolution as low as 6.25 ns. Fluorescently modified DNA was diluted to a final concentration of ~1 nM in 10 mM sodium phosphate buffer, pH 7.0, containing 0-1 M NaCl, 0.1 mM EDTH, and 0.3 mg/ml bovine serum albumin to suppress glass-surface adsorption. DNA samples were transferred onto a microscope slide and covered by a coverslip. Sample temperature was controlled by a custom-built objective heater to be constant at 20°C.

FCS data analysis

Fluctuations in the fluorescence signal $I(t)$ due to diffusion of fluorescent DNA conjugates in and out of the detection volume were analyzed via the second-order autocorrelation function:

$$G(\tau) = \frac{\langle I(t)I(t+\tau)\rangle}{\langle I(t)\rangle^2}, \tag{1}$$

where $\langle\ \rangle$ denotes the time average over the total observation time. Equation 1 can be approximated using a 2D diffusion model for a single species in combination with an exponential decay accounting for intersystem crossing:

$$G(\tau) = \frac{1}{N}\left(1+\frac{\tau}{\tau_D}\right)^{-1}(1+A\exp(-k\tau)), \tag{2}$$

with the number of detected molecules N, characteristic diffusion time τ_D, amplitude A, and rate constant k of an exponential decay defined by intersystem crossing rate and triplet lifetime, as described in (55). The characteristic diffusion time τ_D depends on the dimensions of the detection focus ω_{xy} in the x,y-dimension:

$$\tau_D = \omega_{xy}^2/4D, \tag{3}$$

where D is the diffusion coefficient. The 2D model is valid for detection foci with $\omega_{xy} \ll \omega_z$ (ω_z representing the lateral dimension of the focus), and is of sufficient accuracy to analyze the presented data.

For spherical particles, the diffusion constant D can be expressed in terms of a hydrodynamic radius R_h according to the Stokes-Einstein relation

$$D = k_B T/6\pi\eta R_h, \tag{4}$$

where k_BT is the thermal energy, and η is the solvent viscosity.

MD simulations

All molecular calculations were carried out with the AMBER 8 molecular simulation program package (56). Trajectory analysis was partly accomplished with Visual Molecular Dynamics (57). Trajectories were simulated for polythymine $(dT)_N$, with N = (2, 4, 8, 16, 32, 64, 128), and MR121-labeled polythymines, MR121-$(dT)_N$, of equal length. Further simulations were performed for abasic sites $(dS)_N$, representing the pure backbone of ssDNA, and for penetrable polythymine $(dTpen)_N$, a hypothetical ssDNA that can penetrate itself, since all van der Waals interactions were switched off.

Starting structures were generated from AMBER's residue library allnucleic94.lib with LEAP and energy-minimized with SANDER for a maximum of 10,000 steps using the steepest-descent algorithm for four steps and conjugate gradient thereafter. MD simulations were run with SANDER using the AMBER force field FF99 (58), an integration time of 1 fs, and a nonbonded cutoff of 12 Å. Attractive nonbonded interactions were deactivated using SANDER's NMR refinement options (HB, ELEC, ATTRACT). For the simulation of $(dTpen)_N$, van der Waals interactions were deactivated using SANDER's NMR refinement options (NB). To ensure sufficient sampling of allowed conformations, a simulation temperature of 800 K was chosen. Snapshots were taken from the trajectories every 1 ps starting after the first 250 ps of simulation time. The offset was set to exclude system equilibration (heating up from 0 K to 800 K) and to assure relaxation from the unlikely starting geometry of an extended oligonucleotide. Simulations were carried out over 20,250,000 time steps of 1 fs each, yielding a usable trajectory of 20-ns length. Due to the elongated structure derived from the Leap libraries, AMBER's internal virtual box was sporadically busted, leading to abortion of the simulation. This was overcome by restarting the simulations, with an increased box size, and concatenating the produced trajectories.

Radius of gyration S was calculated for each MD run using Visual Molecular Dynamics for each oligonucleotide length. S, as defined by

$$S^2 = \frac{1}{n}\sum_{i=1}^{n}(\vec{R}_i - \vec{R}_{cm})^2, \tag{5}$$

where $\vec{R}_{cm}$ denotes the center of mass, $\vec{R}_i$ the position of atom i, and n the number of atoms. End-to-end distances R were determined as

$$R^2 = (\vec{R}_{H3T} - \vec{R}_{O5'})^2, \tag{6}$$

where $\vec{R}_{O5'}$ is the position of oxygen atom O5′ in the first nucleic residue and $\vec{R}_{H3T}$ is the position of the capping hydrogen of the last residue's 3′-hydroxyl group. The persistence length L_p was estimated as the orientational correlation length $L_{p,oc}$ (59), which is determined from an exponential fit to the orientational correlation function

$$C_k = \langle\cos\theta_k\rangle = C_0\exp(-kb/L_{p,oc}), \tag{7}$$

where $\langle\cos\theta_k\rangle$ denotes a temporal average over the angles between two virtual P-P bonds separated by k other bonds of length b. Alternatively L_p was estimated as the projection length $L_{p,pro}$ (59):

$$L_{p,pro} = b\sum_k\langle\cos\theta_k\rangle. \tag{8}$$

RESULTS

Experiment

Using FCS, we monitored translational diffusion of polydeoxythymine, MR121-$(dT)_N$, labeled site-specifically with

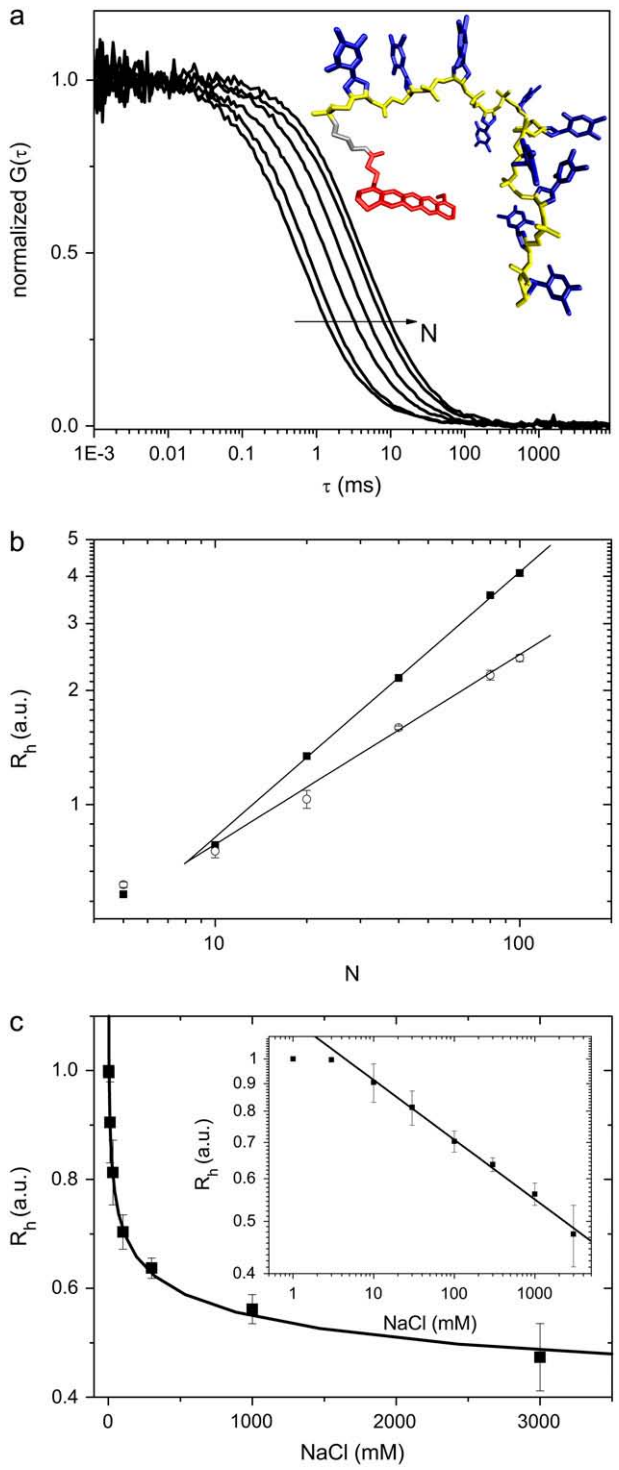

FIGURE 1 Translational diffusion of polythymine measured by FCS. (*a*) Normalized FCS data for MR121-$(dT)_N$ with $N = (5, 10, 20, 40, 80, 100)$ (*left* to *right*). (*Inset*) Random structure of polythymine with the sugar-phosphate backbone (*yellow*), thymine bases (*blue*), and the fluorescent label MR121 attached at the 5′-end (*red*). (*b*) Hydrodynamic radius R_h (proportional to the experimental diffusion time τ_D measured by FCS) of MR121-$(dT)_N$, as determined in aqueous solution with 10 mM (*solid squares*) and 1 M (*open circles*) NaCl. The solid lines represent power-law fits with exponents $\nu = (0.69 \pm 0.01)$ and $\nu = (0.50 \pm 0.02)$ for 10 mM and 1 M NaCl, respectively. Error bars, either shown or on the order of the symbol size, represent the standard deviation of three measurements. (*c*) Hydrodynamic radius R_h of MR121-$(dT)_{100}$ measured by FCS at NaCl concentrations between 1 mM and 3 M. The data reveals a power-law dependence with an exponent of $\alpha = (-0.11 \pm 0.01)$ when displayed and fitted on a double-logarithmic plot (*inset*). Error bars represent standard deviations of three measurements.

the oxazine derivative MR121 at the 5′-end, in aqueous solution (depicted in Fig. 1 *a*). Thymine bases are known to exhibit negligible base-pairing interactions, and the weakest base-stacking interactions compared to all other nucleinbases. Polythymine is known to behave as an unstructured polymer that randomly samples a conformational space depending on its contour length, i.e., the total length along the polymer backbone. We investigated MR121-$(dT)_N$ with various contour lengths by changing N from 5 to 100.

As a fluorescent molecule diffuses through the confocal observation volume, it will emit photons in the red spectral region (emission maximum of MR121 is 673 nm) upon excitation with 633 nm laser light. For a fixed observation volume, which is determined by the laser excitation profile and the detection optics, the observed fluorescence will fluctuate with a characteristic time constant that depends on the diffusion constant of the molecule. Analyzing such fluctuations by calculating the autocorrelation curve of the fluorescence signal yields a time constant that is inversely proportional to the diffusion constant (Eq. 3) and directly proportional to an apparent hydrodynamic radius as defined by the Stokes-Einstein equation (Eq. 4). All observed correlation functions $G(t)$ could be well fitted by the appropriate analytical expression (Eq. 2), independent of polymer size. As we increased the contour length of polythymine, FCS curves were shifted toward longer diffusion times, revealing an increase of the apparent hydrodynamic radius (Fig. 1 *a*).

The accuracy of our diffusion measurements using FCS on a custom-made confocal microscope was determined by estimating the relative standard deviation of repeated measurements (measurement time 100 s, excitation power 50 μW) and found to be ~5% for most of the presented experiments (the accuracy can be improved to <1% using longer measurement times and increased excitation power). All FCS measurements were performed at a concentration of ~1 nM, making intermolecular interactions negligible. A small contribution from photophysical processes was found to be dependent on excitation power (with an amplitude K well below 0.05 at an excitation power of 50 μW (54)), but independent of the investigated sample. Diffusion times were independent of sample concentration and excitation power for excitation powers well below the saturation limit.

Assuming a diffusion constant of $D = 4.26 \times 10^{-6}$ cm^2 s^{-1} for MR121 (as measured for the structurally similar fluorophore Atto655 (60)), we calculated diffusion constants for polythymine to range from $\sim 2.2 \times 10^{-6}$ cm^2 s^{-1} to $\sim 0.4 \times 10^{-6}$ cm^2 s^{-1}. Inverse diffusion constants and, thus,

hydrodynamic radii R_h were observed to scale with contour length (expressed through the number of dT residues N) as $R_h \sim N^{\nu}$ for polynucleotides with >10 residues. Below 10 bases, the influence of the fluorophore on the diffusion time disguises polymer properties. For MR121-$(dT)_N$ with $10 < N < 100$ ν varied between 0.5 (1 M NaCl) and 0.7 (10 mM NaCl) as a function of the ionic strength of the solvent (Fig. 1 *b*).

In Fig. 1 *c*, the dependence of R_h on ionic strength is shown in detail for MR121-$(dT)_{100}$. Ionic strength was changed by varying the concentration of sodium chloride from 0 to 3 M in bidistilled water. Identical results were found in 10 mM phosphate buffer for NaCl concentrations > 10 mM. The hydrodynamic radius scales with ionic strength I as $R_h \sim I^{\alpha}$ with $\alpha = (-0.11 \pm 0.01)$ for NaCl concentrations >10 mM (as visible in a double-logarithmic plot (Fig. 1 *c*, *inset*)). For NaCl concentration <10 mM, R_h saturates at a constant level.

Simulation

To rationalize our results and study the polymer properties of polythymine derivatives in more detail, we performed MD simulations with a focus on geometrical properties, neglecting electrostatic interactions and solvent effects. We sampled the configurational space of polythymine derivatives using an Amber force field that was limited to short-range (van der Waals) interactions in vacuum. The approach constitutes a hard-sphere model of ssDNA in which excluded volume is set by van der Waals radii. By this approach, we explored all constraints on configurational dynamics given by bond length, bond angles, and bond rotations, as well as excluded volume due to steric interactions.

We investigated four different polythymine derivatives: $(dT)_N$, MR121-$(dT)_N$, $(dS)_N$, and $(dTpen)_N$. Simulations of $(dT)_N$ and MR121-$(dT)_N$ were performed to probe the differences between MR121-labeled and nonlabeled polythymine. A polynucleotide made of abasic sites $(dS)_N$, i.e., a sugar-phosphate backbone without attached base moieties (5′-phospho-1,2-dideoxy-α-D-ribose), was investigated to test whether the attached bases have any influence on polymer conformations. A hypothetical polynucleotide, $(dTpen)_N$, that is self-penetrable but consists of the same bond configurations and residues as polythymine, was simulated to identify any excluded-volume effect. The simulation was realized by switching off all van der Waals interactions.

To ensure sufficient sampling, we performed simulations at temperatures ranging from 300 K to 1000 K. At a nominal temperature of 800 K, we observed sufficient sampling of the geometrically allowed conformational space without severe stabilization of individual states due to local energy minima. The temperature was low enough to allow for 1-fs integration steps without producing instabilities.

For each molecule, with contour length fixed by the specified number of residues, we extracted three parameters to characterize the polymer: 1), end-to-end distances R (the distance between the first and last residues of the DNA polymer as defined in Eq. 6); 2), radius of gyration S (the sum over all distances between the actual position of all atoms and the molecule's center of mass (Eq. 5)); and 3), persistence length (Eqs. 7 and 8). Average values of the square end-to-end distances and the radius of gyration were calculated directly from the corresponding distribution functions.

First, we investigated average values of squared end-to-end distances $\langle R^2 \rangle$ and radii of gyration $\langle S \rangle$. We present $\langle R^2 \rangle$ (Fig. 2 *a*) and $\langle S \rangle$ (Fig. 2 *b*) as a function of contour length for the various polymers with 2–128 residues. The double-logarithmic plot shows that $\langle R^2 \rangle$ for all polynucleotides in which van der Waals interactions induce excluded volume scales approximately as $\langle R^2 \rangle \sim N^{\mu}$ with an exponent $\mu > 1$, and thus deviates from the power-law dependence of an ideal polymer ($\mu = 1$). A power-law fit to $\langle R^2 \rangle$ for $(dTpen)_N$ yields an exponent of $\mu = 0.96 \pm 0.01$, and thus confirms the absence of excluded-volume effects. For comparison power-law functions with $\mu = 1$, as expected for an ideal FJC, and $\mu = 2$, as expected for a rigid rod, are shown as solid lines in Fig. 2 *a*. No influence of the attached fluorophore on $\langle R^2 \rangle$ was detected, as data points for MR121-$(dT)_N$ and $(dT)_N$ overlay perfectly. Abasic sites, $(dS)_N$, have slightly reduced $\langle R^2 \rangle$, reflecting a small but significant effect due to steric interactions of base residues.

The plot of $\langle S \rangle$ as a function of N confirms the fluorophore's influence on total polymer dimensions becoming negligible for >~20 residues. $\langle S \rangle$ scales perfectly well for unlabeled polythymine over all sizes with $2 < N < 128$ and follows a power law with exponent 0.62 ± 0.01. This result is in perfect agreement with the experimental observation that the hydrodynamic radius, being proportional to $\langle S \rangle$, scales as a power law for >10–20 residues and deviates for short MR121-$(dT)_N$ in a way similar to $\langle S \rangle$. Overall, the length dependence of $\langle S \rangle$ for labeled polythymine is in excellent agreement with experimental R_h of polythymine in aqueous buffer with 100 mM NaCl (Fig. 2 *c*). The measured power-law exponent of 0.58 ± 0.02 is furthermore in excellent agreement with the theoretical exponent for a polymer in which excluded-volume effects contribute, numerically estimated at 0.588 (1).

The length dependence of the polymer dimension is often visualized through Flory's characteristic ratio $C_N = \langle R^2 \rangle / Nb^2$, where Nb^2 is the average square end-to-end distance of an equivalent FJC. We assumed an equivalent chain with a virtual bond length $b = 0.66$ nm, number of segments N equal to the number of residues, and contour length $L_c = Nb$. We found that C_N strongly increases for all simulated polynucleotides except $(dTpen)_N$ up to ~20 residues, and approaches an asymptotic limit C_∞ between 5 and 6 for $(dT)_N$ and between 3 and 4 for $(dS)_N$ (Fig. 3 *a*). The observation that C_N is length-independent and close to 1 for $(dTpen)_N$ shows that short-range (van der Waals) interactions influence

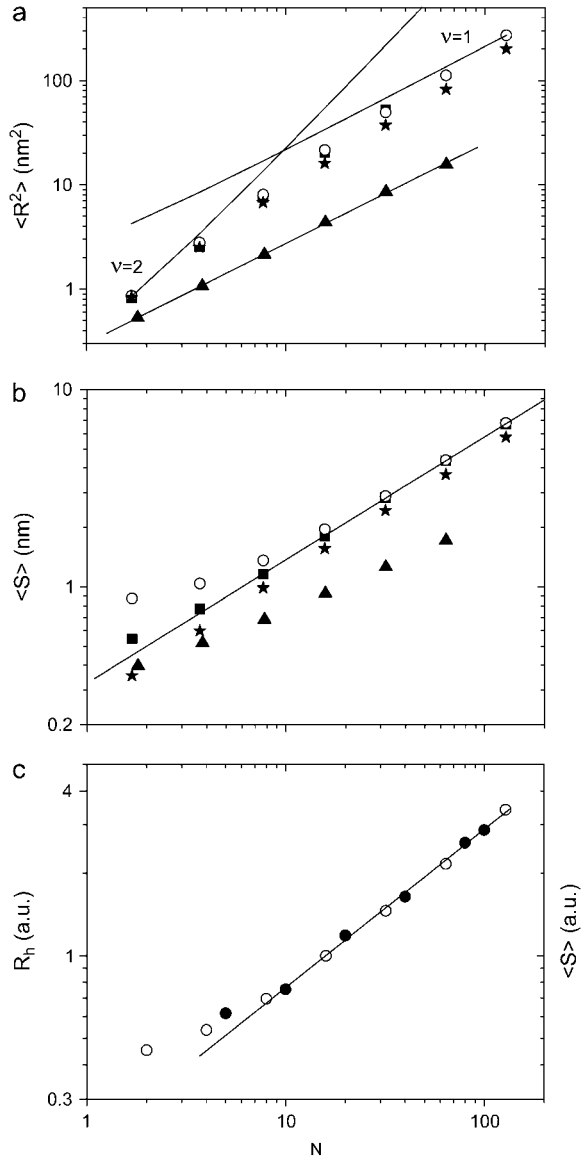

FIGURE 2 Polymer properties of polythymine derivatives determined by MD simulation. (*a*) Average square end-to-end distances $\langle R^2 \rangle$ for polythymine (*solid squares*), MR121-labeled polythymine (*open circles*), polymer of abasic sites (*stars*), and penetrable polythymine (*triangles*). For comparison, solid lines are displayed, representing power laws $\langle R^2 \rangle \sim N^{\mu}$ with exponent $\mu = 1$ (characteristic for an ideal flexible polymer) and $\mu = 2$ (characteristic for a rod). A power-law fit for penetrable polythymine yields an exponent of $\mu = (0.96 \pm 0.01)$. (*b*) Average radius of gyration $\langle S \rangle$ for polythymine (*solid squares*), MR121-labeled polythymine (*open circles*), polymer of abasic sites (*stars*), and penetrable polythymine (*triangles*). A power-law fit to $\langle S \rangle$ of polythymine with $N > 5$ yields an exponent of $\nu = (0.62 \pm 0.01)$ and is displayed as a solid line. (*c*) Hydrodynamic radius R_h (*solid circles*) of MR121-$(dT)_N$ with $N = (5, 10, 20, 40, 80, 100)$ measured using FCS in 100 mM NaCl, and average radii of gyration $\langle S \rangle$ (*open circles*) estimated by MD simulations. The data is scaled such that data points for MR121-$(dT)_{10}$ overlap. The solid line represents a power-law fit to experimental data with $20 < N < 100$, with an exponent of $\nu = (0.58 \pm 0.02)$, in excellent agreement with the prediction of 0.588 for a hypothetical polymer with excluded-volume effects contributing.

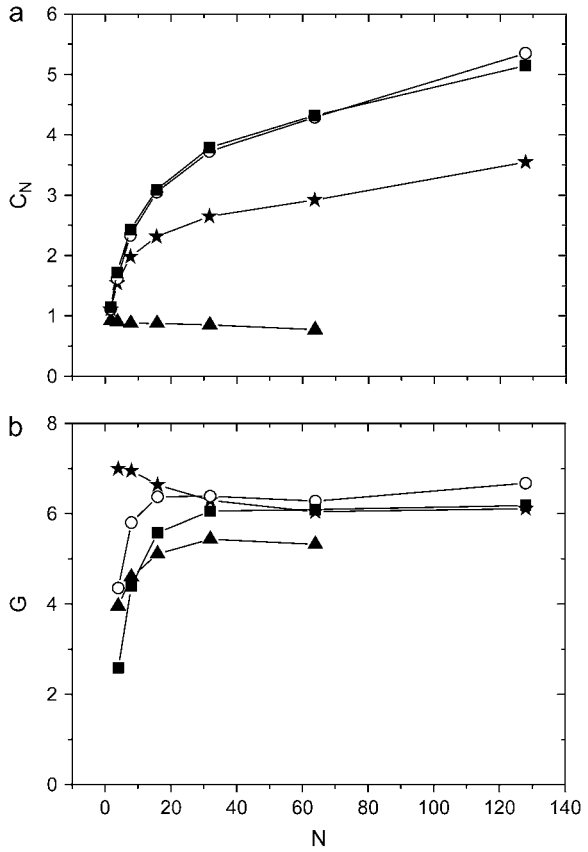

FIGURE 3 Flory's characteristic ratio C_N (*a*) and the structure factor $\langle R^2 \rangle / \langle S^2 \rangle$ (*b*) plotted as a function of N for polythymine (*solid squares*), MR121-labeled polythymine (*open circles*), polymer of abasic sites (*stars*), and penetrable polythymine (*triangles*).

polymer flexibility to a larger degree than do constrained bond angles.

Fig. 3 *b* shows the ratio of average square end-to-end distance and average square radius of gyration, referred to as the structure factor: $G = \langle R^2 \rangle / \langle S^2 \rangle$. G increases with increasing contour length for all polymers except $(dS)_N$ and approaches an asymptotic value between 6 and 7 for $> \sim 20$ residues. The asymptotic value is close to the structure factor of an ideal FJC ($G = 6$; for a rigid rod, $G = 12$) (1,61) and again reflects the fact that ssDNA in the limit of long chains is well described as a polymer with large but not unrestricted flexibility. G values are reduced for shorter polymers, as base residues and MR121 contribute more to $\langle S^2 \rangle$ than they do to $\langle R^2 \rangle$.

In Fig. 4, we show radial distribution functions $G(r)$ of rescaled end-to-end distances r (i.e., R in units of the contour length L_c: $r = R/L_c$) for polynucleotides with $N = (64, 32, 16, 8, 4)$ and for corresponding WLCs. The contour length was estimated by extracting average distances between successive phosphorus atoms in the DNA backbone. We extracted a mean P-P distance for each polymer that is independent of the bond position in a single polynucleotide, and independent of the number of residues N. All P-P

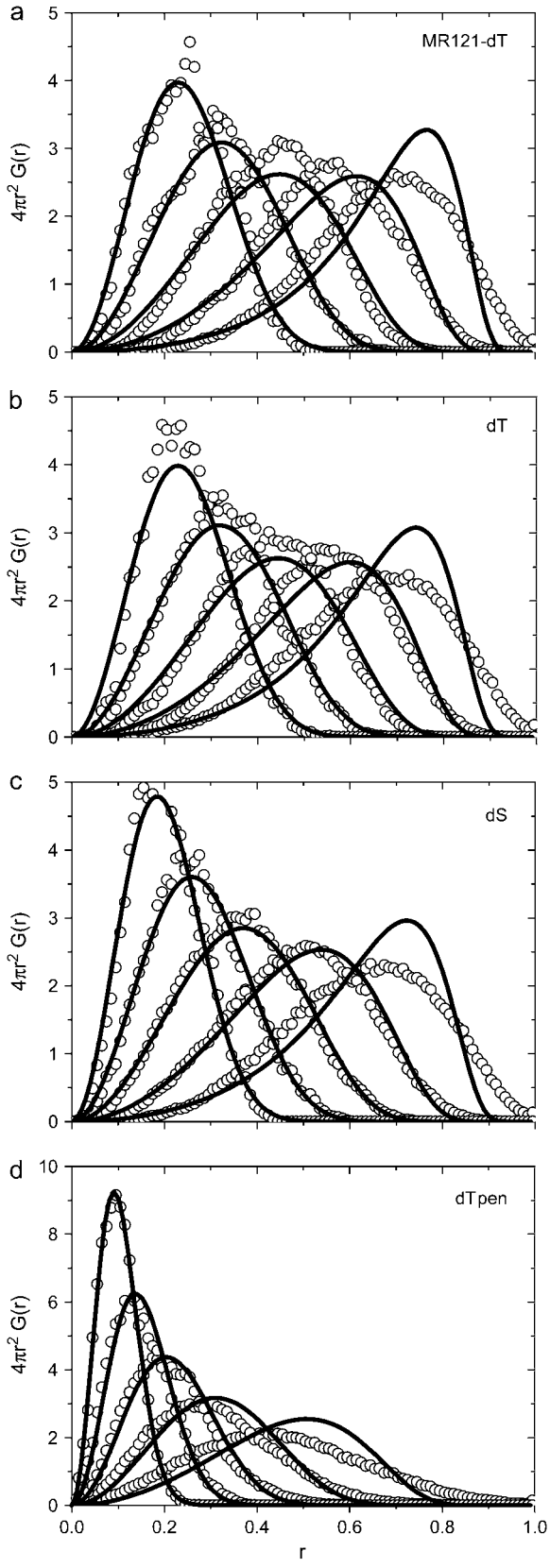

FIGURE 4 Distribution functions $4\pi r^2 G(r)$ of radial, contour-length normalized end-to-end distances r estimated by MD simulations. Distribution functions are shown for MR121-labeled polythymine (*a*), polythymine (*b*), polymer of abasic sites (*c*), and penetrable polythymine (*d*), with 64, 32, 16, 8, and 4 residues, respectively, from left to right. Each distribution is overlaid with a WLC distribution of equal $\langle r^2 \rangle$ adjusted by $t = L_c/L_p$ following Eq. 9. All distributions are normalized to equal integrals.

distances were distributed with a standard deviation of <20% of the mean value. A further partitioning into smaller virtual bonds, e.g., partitioning into the two virtual bonds P-$C_{5'}$ and $C_{5'}$-P, showed no advantage, as relative length fluctuations for the virtual bond $C_{5'}$-P were comparable to those of P-P vectors (and those of P-$C_{5'}$ were naturally much smaller). These results are consistent with earlier calculations by Olson and Flory, who showed that ssDNA can be described as a freely rotating chain with virtual bonds of constant length representing individual P-P vectors (15).

The length of this virtual bond b was 0.66 ± 0.07 nm (mean ± SD), resulting in a contour length of $L_c = bN$ between 1.3 nm ($N = 2$) and 84.5 nm ($N = 128$). To show in which size range and to what degree the simulated distribution function resembles that of a WLC we overlaid simulations with corresponding WLC distribution functions. Correspondence was based on matching contour length and average square end-to-end distance $\langle R^2 \rangle$. WLC distribution functions were calculated using the analytical expression given by Thirumalai and Ha (62). The plots demonstrate that $G(r)$ for polythymine and $G(r)$ for the corresponding WLC show better agreement with increasing contour length, becoming nearly equal for >~30 residues. For $(dS)_N$ and $(dTpen)_N$, simulated and ideal WLC distributions show good agreement for slightly shorter contour lengths of >~10 residues, again reflecting the influence of excluded volume (Fig. 4, *c* and *d*).

Attachment of the fluorescent label MR121 at the 5′ end of the ssDNA has only a weak effect on $G(r)$, as presented in Fig. 4, *a* and *b*, where the simulated end-to-end distances are shown for polythymine with and without MR121 (note that end-to-end distances are calculated from the first nucleic residue's O5′ to the last residue's H3T, neglecting the fluorophore if present).

When plotting distribution functions $P(S)$, where the fluorophore is now included in the calculation of S, a difference between labeled and unlabeled molecules appears (Fig. 5 *a*). The difference is more pronounced for shorter polythymines, as is visible in the $P(S)$ overlay for MR121-$(dT)_N$ and $(dT)_N$ presented in Fig. 5 *a*. Whereas $P(S)$ for short polythymines is considerably broadened and shifted toward larger values upon MR121 attachment, the fluorophore's influence on $P(S)$ decreases with increasing length and becomes insignificant for >~60 thymine residues. Distribution functions are similar in shape for all molecules with four or more residues and resemble a Gaussian distribution with a slight asymmetry.

Last, we estimated the persistence length from simulated data and interpreted the experimental observation of a salt-dependent hydrodynamic radius by an electrostatic persistence

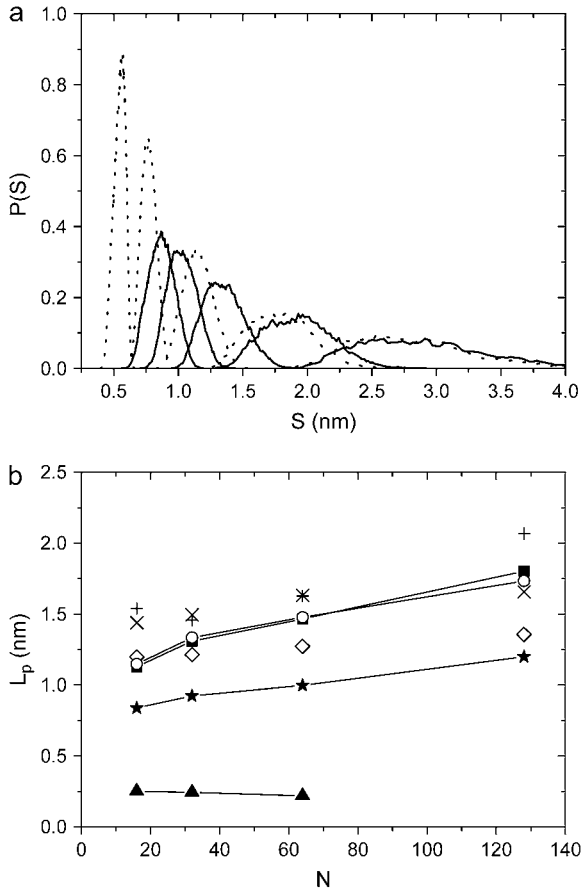

FIGURE 5 (*a*) Distribution functions $P(S)$ of radii of gyration estimated by MD simulations. Distributions functions are plotted for polythymine (*dotted line*) and MR121-labeled polythymine (*solid line*) with 2, 4, 8, 16, and 32 residues, respectively, from left to right. The contribution of the attached fluorophore decreases with increasing polymer length, becoming negligible for MR121-$(dT)_N$ with $N > 16$. All functions are normalized to equal integrals. (*b*) Persistence length L_p was estimated by various means from simulated data: 1), L_p as determined from the corresponding WLC distribution (Fig. 4) is plotted for polythymine (*solid squares*), MR121-labeled polythymine (*open circles*), polymer of abasic sites (*stars*), and penetrable polythymine (*triangles*); 2), L_p as determined by the projection length is plotted for polythymine (X), MR121-labeled polythymine (*plus signs*), and polymer of abasic sites (*diamonds*). The persistence length of penetrable polythymine was too small to be estimated by the projection length.

length that changes with ionic strength. The persistence length can be estimated in multiple ways from simulated data (59): First, we calculated the orientational correlation length $L_{p,oc}$ (Eq. 7) and projection length $L_{p,pro}$ (Eq. 8). We found $L_{p,pro}$ values around 1.5 nm to be weakly dependent on the contour length and slightly smaller for abasic-site polymers. A fit of orientational correlation functions revealed nonexponential decays and thus did not yield reliable $L_{p,oc}$ values. Second, we calculated the persistence length $L_{p,WLC}$ for a WLC model with equal $\langle R^2 \rangle$ and corresponding contour length compared to simulated data. The relation between $\langle R^2 \rangle$, contour length L_c, and persistence length $L_{p,WLC}$ is determined by the following equation (61):

$$\langle R^2 \rangle = 2L_{p,WLC}^2(\exp(-L_c/L_{p,WLC}) - 1 + L_c/L_{p,WLC}). \quad (9)$$

It is important to remember that an increasing deviation between WLC and simulated end-to-end distance distributions was found for chains with $<\sim 30$ residues. This is again reflected in the plot of $L_{p,WLC}$ as a function of contour length (Fig. 5 *b*), where a slight length dependence appears. Overall, we determined a persistence length of ~ 1.7 nm for polythymine $(dT)_{128}$, ~ 1.2 nm for abasic sites $(dS)_{128}$, and ~ 0.2 nm for penetrable polythymine $(dTpen)_{128}$.

We conclude that polythymine with 30–100 residues can be well described as a WLC with respect to geometric and steric constraints.

DISCUSSION

The idea that DNA, both in its double- and single-stranded forms, can be approximated as a semiflexible polymer has found wide acceptance. In particular, the elastic properties of dsDNA are well described by a WLC or FJC model (7). For ssDNA, deviations from WLC behavior were found for low extension at extremely high and low salt concentrations (7,46), effects that were rationalized by intramolecular base pairing and stacking interactions in heterogeneous ssDNA (47,48), or by excluded-volume effects due to short-range van der Waals and long-range electrostatic interactions (46,63).

Our measurements of diffusion time reflect an important polymer property, the radius of gyration, and its dependence on contour length and ionic strength of the solvent. The diffusion time observed in an FCS experiment is inversely proportional to the molecule's diffusion constant. Assuming that the diffusion constant is proportional to an apparent hydrodynamic radius, estimated via the Stokes-Einstein equation, and, furthermore, that the hydrodynamic radius is directly proportional to the molecule's radius of gyration, we can experimentally determine the radius of gyration of polythymine using FCS.

Our results extend the size range for which translational diffusion constants of unstructured ssDNA have been observed toward short contour lengths. They confirm that diffusion constants change with length according to a polymer that is impenetrable due to excluded volume. The degree of excluded volume is dependent on the ionic strength of the solvent, confirming that excluded volume is determined both by steric interactions due to van der Waals forces and by electrostatic interactions. Using MD simulations, we tested how much the observed length dependence originates from excluded-volume effects due to short-range interactions or from reduced backbone flexibility due to steric interactions and constrained bond angles, excluding electrostatic interactions. Based on the simulation result that MR121-$(dT)_N$ with $N > 30$ exhibits distribution functions of end-to-end distances and radii of gyration comparable to those of an ideal WLC, and with negligible influence of the fluorophore, we compared measured diffusion constants to simulated radii of

gyration. Perfect agreement was found for an ionic strength corresponding to 100 mM NaCl at a temperature of 20°C. This result indicates that in 100 mM NaCl solution electrostatic interactions between polythymine residues are perfectly shielded, such that polymer flexibility is entirely restricted by geometrical constraints and excluded volume due to short-range interactions alone.

High-temperature MD simulations in vacuum with a force field limited to short-range interactions probe all conformations that are allowed given the limited degrees of freedom in the sugar-phosphate backbone and steric interactions. These simulations are conceptually very similar to those carried out by Olson and co-workers (14,15,29,30). A comparison between the lengths of various virtual bonds—$C_{5'}$-P, P-$C_{5'}$, and P-P—in our simulations, and as published by Olson, showed agreement within 10%. Since no constraint was made for sugar puckering, we observed two populations in each distance histogram for virtual bonds that contained the $C_{3'}$-$C_{4'}$ bond. The distances agreed well with average bond length estimated for 2′- and 3′-endo conformations (14). A dynamic equilibrium of 2′- and 3′-endo conformations was detected by numerous NMR studies, justifying our analysis. The average length for a P-P virtual bond was consistently found to be 0.66 ± 0.07 nm in all simulations, which is in good agreement with the P-P distance of 0.63 ± 0.08 nm determined by Murphy et al. from various crystal structures of ssDNA complexes (17). However, it should be noted that some experimental evidence exists for P-P distances to be slightly smaller, approaching 0.4 nm (27,64).

We further tested whether the attached bases have any influence on polymer conformations by simulating polynucleotides made of abasic sites. Our results confirm Olson's claim that base residues have a very limited influence on polynucleotide conformations (30). However, we did find a small but significant effect that results in an average square end-to-end distance decreased by ~25% and an average radius of gyration decreased by ~15% for the longest polynucleotide ($N = 128$) in the absence of electrostatic interactions.

Further analyzing simulations for polythymine without a fluorescent label, we were able to demonstrate that the polymer properties become independent of the detailed atomic structure and the limited degrees of freedom when the contour length exceeds ~30 residues. It is important to note that for polythymines with <30 residues a WLC description with respect to end-to-end distribution functions deviates significantly from simulated data due to steric and geometrical constraints alone. Taking electrostatic interactions into consideration, it is possible that deviations from a perfect WLC distribution might appear for even longer polynucleotides. However, there are also regimes in which electrostatic effects only influence the effective persistence length of a corresponding WLC, without changing the functional shape of end-to-end distributions (28).

The most important effect of electrostatic interactions, however, is on static flexibility as expressed through an effective persistence length L_p, Flory's characteristic ratio C_∞, or the structure factor G. Both $G \sim 6$–7 and $C_\infty \sim 5$, which are consistent with previous calculations (45), indicate that polynucleotides are very flexible biopolymers, comparable to the most flexible polypeptides. Flory has shown that polypeptides, with virtual bonds well defined as the connecting vector between adjacent C_α atoms, exhibit C_∞ between 2 and 3 for the most flexible peptides (polyglycine) (65). The main difference lies in the fact that polynucleotides always represent a polyelectrolyte in which static flexibility is strongly influenced by electrostatic interactions. Accordingly, Olson et al. found $C_\infty > 8$ for polynucleotides when taking electrostatic interactions into account (14).

However, as electrostatic interactions are long-range, exact theoretical treatments of realistic systems are rare, and computer simulations are still limited by calculation power. The behavior of a polyelectrolyte is determined by the strength of the interaction between charged segments measured in terms of the Bjerrum length, $l_B = e^2/4\pi\varepsilon k_B T$ (where e is the charge per segment, ε the dielectric constant of the solvent, and $k_B T$ the thermal energy), screening of electrostatic interactions by counterions measured in terms of the Debye screening length, $r_D = 1/\kappa$ (with $\kappa^2 = 4\pi l_B I$ and I representing ionic strength), and a separation distance between charged segments, A. For ssDNA in aqueous solution, $l_B \sim 0.7$ nm, $r_D \sim 0.5$ nm, and $A \sim 0.43$ nm (66). An accurate experimental dependence of persistence length on ionic strength, and thus on electrostatic interactions, could serve as a benchmark for both theory and computer simulations.

We therefore estimated the dependence of an apparent persistence length on the solution ionic strength from measured diffusion times of MR121-$(dT)_{100}$ at various concentrations of NaCl. Squared diffusion times are directly proportional to persistence length under the following conditions: 1), diffusion times τ_D are proportional to an apparent hydrodynamic radius, which itself is proportional to $\langle S \rangle$; 2), $\langle S^2 \rangle$ is proportional to $\langle R^2 \rangle$; and 3), Eq. 9 can be approximated by $\langle R^2 \rangle = 2L_c L_p$, which is true for $L_c/L_p \gg 1$. For $(dT)_{100}$, these conditions are valid within experimental uncertainty and can thus be used to estimate the salt-dependent persistence length of MR121-$(dT)_{100}$. We find $L_p \sim \tau_D^2 \sim I^{2\alpha}$, with $2\alpha = -0.22 \pm 0.01$, changing L_p by a factor of 2 when going from 1 mM to 3 M NaCl. This agrees well with results by Murphy et al. (17).

Taking into account the bare persistence length as estimated from our MD simulations with electrostatic interactions excluded, $L_{p0} \sim 1.7$ nm, a theory estimating the scaling behavior of the persistence length with electrostatic interactions has to be valid for strongly charged, flexible polyelectrolytes with $A \sim (L_{p0} l_B)^{1/2}$, which is not the case for the established OSF theory. Thus, it is not surprising that we find a scaling behavior that is different from $L_p = L_{p0} + I^{-1}$ as predicted by OSF theory and also slightly different from the alternative scaling behavior $L_p = L_{p0} + I^{-0.5}$, as suggested by others (25,26). Our measurements of the scaling law,

however, are in good agreement with estimates derived by Laurence et al. (27). Finally, it should be noted that our estimation of the bare persistence length for polythymine should equal the experimental persistence length as measured in 100 mM NaCl. Previous measurements of ssDNA persistence length in aqueous solution, with an ionic strength approximately corresponding to a monovalent salt concentration of 100 mM, yielded values between 1.3 and 3 nm (16–18,67) and indeed agree very well with our results.

CONCLUSION

We have presented length-dependent diffusion constants of polythymine fluorescently labeled with the oxazine fluorophore MR121 measured by FCS. Single-molecule-sensitive fluorescence spectroscopy allows experiments to be performed at low sample concentrations excluding intermolecular interactions. Depending on the ionic strength of the solvent, inverse diffusion constants, which can be interpreted as hydrodynamic radius, scale with the polymer's contour length (i.e., approximately the number of bases N times the distance between adjacent phosphorus atoms b) as N^{ν}, with ν between 0.5 and 0.7. MD simulations in vacuum, with a force field restricted to short-range van der Waals interactions, reveal that the simulated radius of gyration scales with contour length, in agreement with a semiflexible polymer model taking excluded volume into account ($\nu = 0.588$). Comparison between simulated and experimental radius of gyration indicates that electrostatic interactions are completely shielded in the experiment at a monovalent salt concentration of 100 mM. Simulations further show that 1), the fluorophore's influence on the radius of gyration and other polymer properties is negligible for polythymines with $>\sim$30 residues; 2), polythymines with $>\sim$30 residues can be described as a WLC with respect to end-to-end distance distributions; 3), steric hindrance due to base residues has a small effect on static flexibility; and 4), a structure factor of 6–7, a characteristic ratio according to Flory of 5–6, and a persistence length of 1.7 nm reveal limited static flexibility imposed by geometrical constraints and steric interactions. Assuming a WLC behavior, we determined that the experimental persistence length from salt-dependent diffusion measurements scales with ionic strength as $L_p \sim I^{2\alpha}$ with $2\alpha = -0.22 \pm 0.01$, which is in contrast to all existing theories.

Our results yield an experimental confirmation that polythymine with a few tens of residues resembles an unstructured polyelectrolyte that can be described as a semiflexible polymer. The length scaling of the apparent persistence length provides an important experimental result for verification of polyelectrolyte theories and can thus help to develop a complete and accurate description of ssDNA.

We thank K. H. Drexhage for providing the oxazine derivative MR121. We thank Ted A. Laurence, Hannes Neuweiler, and Isabella Daidone for comments on the manuscript and helpful discussions.

Financial support from the Deutsche Forschungsgemeinschaft (SFB 613) is gratefully acknowledged.

REFERENCES

1. Flory, P. J. 1969. Statistical Mechanics of Chain Molecules. Hanser, Munich.
2. Kratky, O., and G. Porod. 1949. Röntgenuntersuchung gelöster Fadenmoleküle. *Recl Trav Chim Pay B*. 68:1106–1122.
3. DeGennes, P. G. 1979. Scaling Concepts in Polymer PhysicsCornell University Press,. Ithaca, NY.
4. Doi, M. 1996. Introduction to Polymer Dynamics. Oxford University Press, Oxford, UK.
5. Doi, M., and S. F. Edwards. 1988. The Theory of Polymer Dynamics. Clarendon Press/Oxford University Press, Oxford, UK.
6. Bustamante, C., Z. Bryant, and S. B. Smith. 2003. Ten years of tension: single-molecule DNA mechanics. *Nature*. 421:423–427.
7. Smith, S. B., Y. Cui, and C. Bustamante. 1996. Overstretching B-DNA: the elastic response of individual double-stranded and single-stranded DNA molecules. *Science*. 271:795–799.
8. Hagerman, P. J. 1988. Flexibility of DNA. *Annu. Rev. Biophys. Biomol. Struct.* 17:265–286.
9. Hagerman, P. J. 1997. Flexibility of RNA. *Annu. Rev. Biophys. Biomol. Struct.* 26:139–156.
10. Yanagida, T., M. Nakase, K. Nishiyama, and F. Oosawa. 1984. Direct observation of motion of single F-actin filaments in the presence of myosin. *Nature*. 307:58–60.
11. Le Goff, L. C., O. Hallatschek, E. Frey, and F. O. Amblard. 2002. Tracer studies on F-actin fluctuations. *Phys. Rev. Lett.* 89:258101.
12. Pampaloni, F., G. Lattanzi, A. Jonas, T. Surrey, E. Frey, and E.-L. Florin. 2006. Thermal fluctuations of grafted microtubules provide evidence of a length-dependent persistence length. *Proc. Natl. Acad. Sci. USA*. 103:10248–10253.
13. Gittes, F., B. Mickey, J. Nettleton, and J. Howard. 1993. Flexural rigidity of microtubules and actin filaments measured from thermal fluctuations in shape. *J. Cell Biol.* 120:923–934.
14. Olson, W. K. 1975. Configurational statistics of polynucleotide chains. A single virtual bond treatment. *Macromolecules*. 8:272–275.
15. Olson, W. K., and P. J. Flory. 1972. Spatial configurations of polynucleotide chains. 3. Polydeoxyribonucleotides. *Biopolymers*. 11: 57–66.
16. Mills, J. B., E. Vacano, and P. J. Hagerman. 1999. Flexibility of single-stranded DNA: use of gapped duplex helices to determine the persistence lengths of Poly(dT) and Poly(dA). *J. Mol. Biol.* 285: 245–257.
17. Murphy, M. C., I. Rasnik, W. Cheng, T. M. Lohman, and T. Ha. 2004. Probing single-stranded DNA conformational flexibility using fluorescence spectroscopy. *Biophys. J.* 86:2530–2537.
18. Kuznetsov, S. V., Y. Shen, A. S. Benight, and A. Ansari. 2001. A semiflexible polymer model applied to loop formation in DNA hairpins. *Biophys. J.* 81:2864–2875.
19. Klimov, D. K., and D. Thirumalai. 2002. Stiffness of the distal loop restricts the structural heterogeneity of the transition state ensemble in SH3 domains. *J. Mol. Biol.* 317:721–737.
20. Lapidus, L. J., P. J. Steinbach, W. A. Eaton, A. Szabo, and J. Hofrichter. 2002. Effects of chain stiffness on the dynamics of loop formation in polypeptides. Appendix: Testing a 1-dimensional diffusion model for peptide dynamics. *J. Phys. Chem. B*. 106:11628–11640.
21. Zhou, H. X. 2001. Loops in proteins can be modeled as worm-like chains. *J. Phys. Chem. B*. 105:6763–6766.
22. Odijk, T. 1977. Polyelectrolytes near the rod limit. *J. Polym. Sci. Polym. Phys.* 15:477–483.
23. Skolnick, J., and M. Fixman. 1977. Electrostatic persistence length of a wormlike polyelectrolyte. *Macromolecules*. 10:944–948.

24. Everaers, R., A. Milchev, and V. Yamakov. 2002. The electrostatic persistence length of polymers beyond the OSF limit. *Eur. Phys. J. E Soft Matter*. 8:3–14.
25. Barrat, J. L., and J. F. Joanny. 1993. Persistence length of polyelectrolyte chains. *Europhys. Lett.* 24:333–338.
26. Ha, B., and D. Thirumalai. 1995. Electrostatic persistence length of a polyelectrolyte chain. *Macromolecules.* 28:577–581.
27. Laurence, T. A., X. Kong, M. Jäger, and S. Weiss. 2005. Probing structural heterogeneities and fluctuations of nucleic acids and denatured proteins. *Proc. Natl. Acad. Sci. USA*. 102:17348–17353.
28. Zandi, R., J. Rudnick, and R. Golestanian. 2002. Radial distribution function of rod-like polyelectrolytes. *Eur. Phys. J. E Soft Matter*. 9: 41–46.
29. Olson, W. K., and P. J. Flory. 1972. Spatial configurations of polynucleotide chains. I. Steric interactions in polyribonucleotides: a virtual bond model. *Biopolymers*. 11:1–23.
30. Olson, W. K., and P. J. Flory. 1972. Spatial configuration of polynucleotide chains. II. Conformational energies and the average dimensions of polyribonucleotides. *Biopolymers*. 11:25–56.
31. Bader, J. S., R. W. Hammond, S. A. Henck, M. W. Deem, G. A. McDermott, J. M. Bustillo, J. W. Simpson, G. T. Mulhern, and J. M. Rothberg. 1999. DNA transport by a micromachined Brownian ratchet device. *Proc. Natl. Acad. Sci. USA*. 96:13165–13169.
32. Tatarkova, S. A., and D. A. Berk. 2005. Probing single DNA mobility with fluorescence correlation microscopy. *Phys. Rev. E Stat. Nonlin. Soft Matter Phys.* 71:041913.
33. Fitzkee, N. C., and G. D. Rose. 2004. Reassessing random-coil statistics in unfolded proteins. *Proc. Natl. Acad. Sci. USA*. 101:12497–12502.
34. Kohn, J. E., I. S. Millett, J. Jacob, B. Zagrovic, T. M. Dillon, N. Cingel, R. S. Dothager, S. Seifert, P. Thiyagarajan, T. R. Sosnick, M. Z. Hasan, V. S. Pande, I. Ruczinski, S. Doniach, and K. W. Plaxco. 2004. Random-coil behavior and the dimensions of chemically unfolded proteins. *Proc. Natl. Acad. Sci. USA*. 101:12491–12496.
35. Smith, D. E., T. T. Perkins, and S. Chu. 1996. Dynamical scaling of DNA diffusion coefficients. *Macromolecules.* 29:1372–1373.
36. Yamakawa, H. 1971. Modern Theory of Polymer Solutions. Harper & Row, New York.
37. Sorlie, S. S., and R. Pecora. 1990. A dynamic light-scattering study of 4 DNA restriction fragments. *Macromolecules.* 23:487–497.
38. Lukacs, G. L., P. Haggie, O. Seksek, D. Lechardeur, N. Freedman, and A. S. Verkman. 2000. Size-dependent DNA mobility in cytoplasm and nucleus. *J. Biol. Chem.* 275:1625–1629.
39. Mandelkern, M., J. G. Elias, D. Eden, and D. M. Crothers. 1981. The dimensions of DNA in solution. *J. Mol. Biol.* 152:153–161.
40. Tirado, M. M., C. L. Martínez, and J. G. de la Torre. 1984. Comparison of theories for the translational and rotational diffusion coefficients of rod-like macromolecules. Application to short DNA fragments. *J. Chem. Phys.* 81:2047–2052.
41. Eimer, W., and R. Pecora. 1990. Rotational and translational diffusion of short rodlike molecules in solution. *Oligonucleotides. J. Chem. Phys.* 94:2324–2329.
42. Tsay, J. M., S. Doose, and S. Weiss. 2006. Rotational and translational diffusion of peptide-coated CdSe/CdS/ZnS nanorods studied by fluorescence correlation spectroscopy. *J. Am. Chem. Soc.* 128:1639–1647.
43. Schaper, A., C. Urbanke, and G. Maass. 1991. Salt dependent changes in structure and dynamics of circular single stranded DNA of filamentous phages of *Escherichia coli*. *J. Biomol. Struct. Dyn.* 8:1211–1232.
44. Wilson, D. H., H. L. Price, J. Henderson, S. Hanlon, and A. S. Benight. 1990. Structure and dynamics of M13mp19 circular single-strand DNA: effects of ionic strength. *Biopolymers.* 29:357–376.
45. Deniz, A. A., T. A. Laurence, M. Dahan, D. S. Chemla, P. G. Schultz, and S. Weiss. 2001. Ratiometric single-molecule studies of freely diffusing biomolecules. *Annu. Rev. Biophys. Biomol. Struct.* V52:233–253.
46. Dessinges, M. N., B. Maier, Y. Zhang, M. Peliti, D. Bensimon, and V. Croquette. 2002. Stretching single stranded DNA, a model polyelectrolyte. *Phys. Rev. Lett.* 89:248102.
47. Maier, B., D. Bensimon, and V. Croquette. 2000. Replication by a single DNA polymerase of a stretched single-stranded DNA. *Proc. Natl. Acad. Sci. USA*. 97:12002–12007.
48. Montanari, A., and M. Mezard. 2001. Hairpin formation and elongation of biomolecules. *Phys. Rev. Lett.* 86:2178–2181.
49. Neuweiler, H., M. Löllmann, S. Doose, and M. Sauer. 2006. Dynamics of unfolded polypeptide chains in crowded environment studied by fluorescence correlation spectroscopy. *J. Mol. Biol.* 365:856–869.
50. Krieger, F., B. Fierz, O. Bieri, M. Drewello, and T. Kiefhaber. 2003. Dynamics of unfolded polypeptide chains as model for the earliest steps in protein folding. *J. Mol. Biol.* 332:265–274.
51. Reference deleted in proof.
52. Shen, Y. Q., S. V. Kuznetsov, and A. Ansari. 2001. Loop dependence of the dynamics of DNA hairpins. *J. Phys. Chem. B*. 105:12202–12211.
53. Heinlein, T., J. P. Knemeyer, O. Piestert, and M. Sauer. 2003. Photoinduced electron transfer between fluorescent dyes and guanosine residues in DNA-hairpins. *J. Phys. Chem. B*. 107:7957–7964.
54. Kim, J., S. Doose, H. Neuweiler, and M. Sauer. 2006. The initial step of DNA hairpin folding: a kinetic analysis using fluorescence correlation spectroscopy. *Nucleic Acids Res.* 34:2516–2527.
55. Widengren, J., U. Mets, and R. Rigler. 1995. Fluorescence correlation spectroscopy of triplet states in solution: a theoretical and experimental study. *J. Phys. Chem.* 99:13368–13379.
56. Case, D. A., T. A. Darden, T. E. Cheatham III, C. L. Simmerling, J. Wang, R. E. Duke, R. Luo, K. M. Merz, B. Wang, D. A. Pearlman, M. Crowley, S. Brozell, V. Tsui, H. Gohlke, J. Mongan, V. Hornak, G. Cui, P. Beroza, C. Schafmeister, J. W. Caldwell, W. S. Ross, and P. A. Kollman. 2004. AMBER 8. University of California, San Fransico.
57. Humpfrey, W., A. Dalke, and K. Schulten. 1996. VMD: visual molecular dynamics. *J. Mol. Graph.* 14:33–38.
58. Wang, J. M., P. Cieplak, and P. A. Kollman. 2000. How well does a restrained electrostatic potential (RESP) model perform in calculating conformational energies of organic and biological molecules? *J. Comput. Chem.* 21:1049–1074.
59. Ullner, M., and C. E. Woodward. 2002. Orientational correlation function and persistence lengths of flexible polyelectrolytes. *Macromolecules.* 35:1437–1445.
60. Dertinger, T., V. Pacheco, I. von der Hocht, R. Hartmann, I. Gregor, and J. Enderlein. 2007. Two-focus fluorescence correlation spectrsocopy: a new tool for accurate and absolute diffusion measurements. *ChemPhysChem*. In press.
61. Benoit, H., and P. Doty. 1953. Light scattering from non-Gaussian chains. *J. Phys. Chem.* 57:958–963.
62. Thirumalai, D., and B. Y. Ha. 1998. Statistical mechanics of semiflexible chains. *In* Theoretical and Mathematical Models in Polymer Research. A. Grosberg, editor. Academic Press, San Diego. 1–35.
63. Bustamante, C., S. B. Smith, J. Liphardt, and D. Smith. 2000. Single-molecule studies of DNA mechanics. *Curr. Opin. Struct. Biol.* 10:279–285.
64. Hingerty, B. E., S. B. Broyde, and W. K. Olson. 1982. The poly(rU) coil: A minimum-energy model that matches experimental observations. *Biopolymers.* 21:1167–1188.
65. Brant, D. A., and P. J. Flory. 1965. The configuration of random polypeptide chains. II. *Theory. J. Am. Chem. Soc.* 87:2791–2800.
66. Stellwagen, E., Y. Lu, and N. C. Stellwagen. 2003. Unified description of electrophoresis and diffusion for DNA and other polyions. *Biochemistry.* 42:11745–11750.
67. Rivetti, C., C. Walker, and C. Bustamante. 1998. Polymer chain statistics and conformational analysis of DNA molecules with bends or sections of different flexibility. *J. Mol. Biol.* 280:41–59.